2017 IEEE International Conference on Robotics and Automation (ICRA)
Singapore, May 29 - June 3, 2017

Pneumatic Reel Actuator: Design, Modeling, and Implementation

Zachary M. Hammond, Nathan S. Usevitch, Elliot W. Hawkes, and Sean Follmer

Abstract— **We present the design, modeling, and implementation of a novel pneumatic actuator, the Pneumatic Reel Actuator (PRA). The PRA is highly extensible, lightweight, capable of operating in compression and tension, compliant, and inexpensive. An initial prototype of the PRA can reach extension ratios greater than 16:1, has a force-to-weight ratio over 28:1, reach speeds of 0.87 meters per second, and can be constructed with parts totaling less than $4 USD. We have developed a model describing the actuator and have conducted experiments characterizing the actuator's performance in regards to force, extension, pressure, and speed. We have implemented two parallel robotic applications in the form of a three degree of freedom robot arm and a tetrahedral robot.**

I. Introduction

Self-deformable modular robotics is a class of modular robotic systems that achieves reconfiguration through the deformation of a fixed topology of modules [1], [2], [3]. Heterogeneous robotic systems comprised of a mesh of linear actuators interconnected at nodes could possess interesting shape changing abilities with wide ranging applications. Such a system could be used in space exploration and search and rescue operations to maintain mobility in irregular terrain and access small spaces for exploration and storage [4], [5], [6]. Furthermore, large deformation could enable the system to perform tasks dependent on shape change such as forming dynamic and self-erecting architecture, camouflaging by mimicking local topography, and interaction with humans by forming useful objects like ramps, stairs, tables, or chairs. Interaction with humans could also take the form of a volumetric shape display that can physically mimic desired objects or digital information. A device offering tangible interactions with digital objects, conceptualized as Digital Clay, has applications in Computer-Aided Design (CAD), 3D printing, and virtual and augmented reality [7]. An interactive shape display of this type would need to be lightweight and compliant to ensure safe interactions with humans. Limitations in high extension actuation utilized in self-deformable systems has constrained the ability for significant shape change necessary for these possible applications.

In order to create a self-deformable system with large shape changing abilities, it is necessary to use an actuator that is highly extensible, lightweight, capable of operating in compression and tension, compliant, and inexpensive. A number of actuators with some of these characteristics exist in the literature.

The authors are with the Dept. of Mechanical Engineering, Stanford University, Stanford, CA 94305, USA zhammond@stanford.edu
This work is supported in part by the National Science Foundation Award # 1637446.

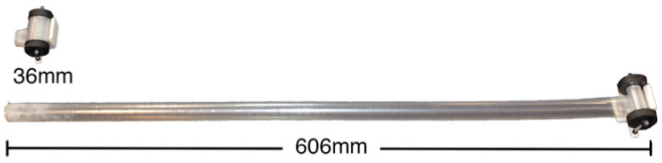

Fig. 1. The PRA is shown here in its contracted form and its extended form.

Perhaps the most prevalent class of compliant actuators is the Pneumatic Artificial Muscle (PAM), which constitutes a soft bladder that contracts as it is pressurized [8]. The McKibben muscle is one form of the PAM that has been widely adopted in robotics and automation applications because of its high force to weight ratio, high speeds, and compliance [8], [9], [10], [11]. However, the PAM does not meet our criteria because they are only effective in tension and are limited to less than a 2:1 extension ratio [8]. The Inverse Pneumatic Artificial Muscle (IPAM) was recently proposed as a high strain variant of the PAM that extends as pressure is increased [12]. The IPAM consists of a thin rubber tubing wrapped helically with inextensible fiber. The IPAM boasts a 4:1 extension ratio while maintaining the high force per weight ratio, high speed, and compliance of the traditional PAM. However, also like the PAM, the IPAM is only effective in tension and does not offer a significant improvement in extension ratio compared to actuators currently utilized in self-deformable robots [4], [5], [6].

Another class of relevant high extension actuators erects columns of varying height by interlocking one or more bands of rigid material together. While the actuators in this class are not compliant, their ability to achieve high extension ratios is compelling. One actuator of this type is the Spiralift, which builds a circular column with two bands of steel [13]. One band is a horizontal spiral with perforated edges and the other is a coil with teeth on the outer edge. A rotary mechanism guides the spiral band along a helical path that aligns the perforations of adjacent turns. The two adjacent turns are then mechanically interlocked by the teeth in the other band, which slide through the perforations. These actuators are capable of extension ratios of 12.5:1, but are very heavy, expensive, and slow. A conceptually similar actuator called the Spiral Zipper builds a circular column from a single band of plastic that mechanically couples to itself [14]. Spiral Zippers with extension ratios of 14:1 have been built and they are lightweight due to the plastic construction, yet they are also unsuitable for this application because they are primarily designed for compression. The last actuator of this class is the Zippermast. The Zippermast forms a triangular column by interlocking three bands of steel that are separately stored

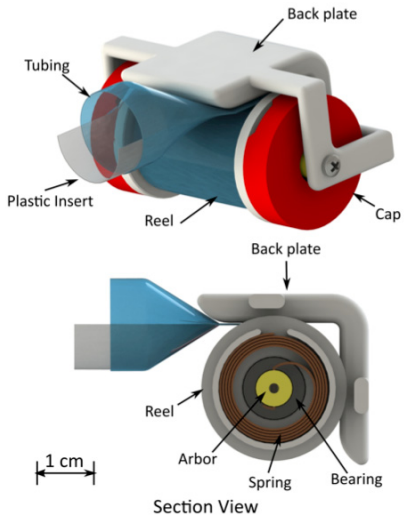

Fig. 2. *Top:* CAD of the PRA. *Bottom:* Section view showing the internal components underneath the cap.

on reels [15]. This actuator can reach extensions up to 32:1, but requires a complex mechanism and has a limited force to weight ratio.

Although the party horn and the Rolatube are not actuators, they are interesting length changing devices. The party horn is a common commodity comprised of a paper tube rolled into a coil that unrolls when air is blown into it. The Rolatube is a bi-stable composite that is stable in the form of a circular beam or a tightly wrapped spiral [16]. It is naturally biased to bend about its long axis causing it to form a long circular beam. When it is forced to bend about the short axis, it forms a roll that occupies a small amount of space for storage. These concepts have inspired our design of the PRA.

While each of these related devices excel at one or more of the qualities that we believe are necessary for an interactive, self-deformable system with large shape changing abilities, we have not found an actuator that meets all of the requirements. Accordingly, we propose the Pneumatic Reel Actuator that is highly extensible, lightweight, capable of operating in compression and tension, compliant, and inexpensive. A prototype of the PRA is displayed in Fig. 1. Our prototypes of the PRA that we present here can reach extension ratios as high as 16.8:1, with a force-to-weight ratio of 28.3:1, reach speeds of 0.89 meters per second, and constructed with parts totaling in cost less $4 USD.

II. Design

The prototype of the pneumatic reel actuator presented in this work was designed to be fabricated on a 3D printer. This fabrication method was chosen to make the procurement of such an actuator easy and inexpensive in small quantities. Two versions of the PRA were designed, but posses many similarities. The first prototype, printed with a Makerbot, was designed to be as inexpensive and simple as possible. The second version contains ball bearings in the revolute joint and is printed with a Projet. The second version was designed to limit non-idealities from sources of friction.

TABLE I
Actuator Specifications

Metric	Without bearings	With bearings
Reel Radius [mm]	9.5	14
Dimensions [mm]	57.4 x 36 x 27.5	55.5 x 38 x 29.5
Cost [USD]	3.95	24.26
Assembly Time [min]	15	30
Plastic Insert Material	Polyester	
Tubing Material	Low Density Polyethylene	
Tubing Radius [mm]	8	
Spring Length [mm]	508	
Spring Thickness [mm]	0.127	
Spring Width [mm]	3.94	

The PRA prototype was constructed with four unique custom parts, as displayed in Fig. 2. The reel includes features to spool flat tubing, house a pair of ball bearings, and house a pair of spiral torsion springs. The back plate prevents the tubing from unraveling and guides the tubing on and off of the reel. The arbor transfers the rotational motion of the back plate with respect to the reel to the torsion springs. The cap restricts the motion of the torsion springs and prevents debris from entering the actuator. Table I lists the actuator specifications.

When the actuator is unpressurized, the springs inside the reel freely retract the tubing, winding it around the reel. As air enters the tubing from the end opposite of the reel, the flexible, but mostly inextensible, membrane of the tubing forms into a cylindrical beam with significantly increased stiffness. As the volume of air inside the actuator rises, more of the tubing is pulled out of the reel to form the beam - lengthening the actuator and storing energy in the torsion springs. As the volume of air decreases, the springs wind the slack tubing back onto the reel and the actuator shortens.

A thin sheet of plastic is added inside the tubing for increased rigidity. When the tubing is deflated, the tubing and the insert can wrap flat around the reel. However, as the tubing inflates, the insert is bent into a half circle. This change of shape increases the second moment of area of the insert and stiffens the actuator.

While other pneumatic actuators rely on the linear deformation of the structural material of the actuator, the tubing of the PRA does not endure significant strain. Instead, the flexure of the torsion spring tightly stored inside the reel accounts for the linear expansion of the actuators tubing. It is for this reason that the PRA is capable of reaching much larger extension ratios than other pneumatic actuators.

III. Actuator Model

The goal of this section is to present an analytical model of the actuator that can be used for actuator design. The model allows geometric parameters of the actuator to be chosen in order to meet performance goals.

A. Energy Balance

The length of the PRA in quasi-static equilibrium will be predominantly driven by the external load on the actuator, the pressure of the air within the actuator, and the stiffness

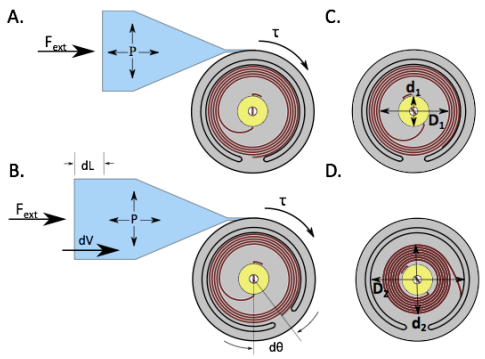

Fig. 3. **A.** A partially inflated PRA experiencing an external force and spring torque. **B.** A small amount of air added to the PRA increases the volume resulting in a length change and a rotation of the spring. **C.** When the PRA is fully retracted, the spring is unwound against the casing. **D.** The spring will wind towards the arbor until it is tightly wrapped around it.

of the spring (Fig. 3A and 3B). Consider an actuator with a spring torque, τ, at an internal pressure, P, that is acted upon by an external force, F_{ext}. Over an infinitesimal time interval, dt, the volume of the actuator is changed by dV resulting in a change of length of the actuator, dL, and a rotation of the reel, $d\theta$. The resulting energy balance can be written as the following:

$$F_{ext}dL + \tau d\theta = PdV \tag{1}$$

Considering small deformations of the PRA, the following substitution may be made:

$$dV = AdL = \pi R^2 dL \tag{2}$$

$$d\theta = -dL/r \tag{3}$$

$$\tau = F_{spring} r \tag{4}$$

where R is the radius of the tubing and r is the radius of the reel. Equation (1) can now be rewritten as:

$$F_{ext} = P\pi R^2 - F_{spring} \tag{5}$$

It should be noted that (5) was derived by neglecting some minor terms in the energy balance. A small amount of energy may be stored in the elastic deformation of the tubing and the plastic insert. The membrane of the tubing will deform slightly as it is pressurized. The plastic insert, which is nominally planar, will store energy as it is bent into a semicircular arc along its length in the inflated beam region and bent into a spiral around the reel. As the actuator changes length, a small segment of the plastic insert will transition from being bent along its length to being bent around the reel. Energy may also be lost to friction generated by moving parts within the reel. These moving parts include the revolute joint, the springs moving against themselves and their housing, and the tubing sliding along the back plate.

B. Spiral Torsion Spring

The behavior of spiral torsion springs has been well documented [17]. For spiral torsion springs with constant, rectangular cross-section, a large number of turns, and clamped endpoints, the output torque and the maximum stress within the spring can respectively be written as:

$$\tau = \frac{Ebh^3}{12l}\theta = \kappa\theta \tag{6}$$

$$\sigma_{spring} = \frac{6}{bh^2} \tag{7}$$

where b is the width of the spring, h is the thickness of the spring, and l is the length of the spring. Equations (6) and (7) were derived assuming zero contact between adjacent turns of the actuator and any housing necessary to contain the spring. Therefore, these equations represent an ideal maximum.

Similar to the mainspring of a watch, the spiral torsion spring in the PRA is constrained inside a hollow case, where the adjacent turns of the spring may contact each other as it winds away from the case towards the arbor. As a result, the torque delivered in response to an angle deformation is analytically uncertain. However, it is possible to calculate the maximum number of turns the spring can support. With a geometry as specified by Fig. 3C and 3D, the maximum number of turns the spring of length can be defined as:

$$n = k\frac{\sqrt{\frac{4}{\pi}lh + d_1^2} + \sqrt{D_2^2 - \frac{4}{\pi}lh} - (D_2 + d_1)}{2h} \tag{8}$$

In the equation above, k is a correction factor less than unity that corrects for the part of the spring that connects to the arbor and the case, which were neglected in the derivation of the equation.

C. Spring Force as a Function of Length

Expressing the force contribution from the spring as a function of actuator length rather than angle is more sensible because the actuator length is more likely the controlled output variable. This force will be a function of the torque generated by the springs, as described above, and the radius of the reel. The radius of the reel changes as the tubing is unwound from the reel. A reel with a nominal radius, r_0, wrapped N times with tubing with total thickness, T, will have an effective radius, r, of:

$$r = r_0 + TN \tag{9}$$

N can be expressed as:

$$N = \frac{L_{total} - L}{\pi(r + r_0)} \tag{10}$$

Solving for r we obtain:

$$r = \sqrt{r_0^2 + \frac{T}{\pi}(L_{total} - L)} \tag{11}$$

and,

$$r_{max} = \sqrt{r_0^2 + \frac{T}{\pi}L_{total}} \tag{12}$$

The spring force can now be described by:

$$F_{spring} = \frac{\kappa L}{r_0^2 + \frac{T}{\pi}(L_{total} - L)} \tag{13}$$

$$F_{spring} \approx \frac{\kappa}{r_{max}^2} L \text{ when } \frac{TL}{\pi} \ll r_{max}^2 \tag{14}$$

Equations (8), (9), and (10) can also be reorganized to solve for the maximum length, L_{max}, when $N = n$:

$$L_{max} = n\pi(2r_0 + Tn) \tag{15}$$

D. Beam Stiffness

In addition to the quasi-static energy balance, understanding the stiffness of the inflated beam and the accompanying stresses within the membrane is essential to the design of a PRA. The stresses developed within the membrane of the pressurized beam without an external load can be described as:

$$\sigma_\theta = \frac{Pr}{t} \tag{16}$$

$$\sigma_z = \frac{Pr}{2t} \tag{17}$$

$$\sigma_r = P \tag{18}$$

where σ_θ is the hoop stress, σ_z is the axial stress, and σ_r is the radial stress [18].

Thin membranes, like the one that comprises the wall of the tubing, possess bending and buckling stiffnesses far below that of the inflated beam [19]. Therefore, the inflated cylinder depends on internal pressure for its load carrying ability. As a load is applied to an inflated cylindrical beam, wrinkles within the membrane begin to form. It is the propagation of this wrinkling phenomenon that reduces the load bearing capability.

Fichter achieved linearized equations that included the effect of pressure on inflated beams under compressive axial force [20]. He shows that the critical load to cause buckling in a pin-end beam column under a compressive axial force can be expressed as:

$$F_{cr} = EI\frac{\pi^2}{L^2}\frac{P + G\pi Rt}{EI\frac{\pi^2}{L^2} + P + G\pi Rt} \tag{19}$$

In the equation above, E is the the elastic modulus, I is the second moment of area, L is the beam length, P is the axial force due to internal pressure, G is the shear modulus, and t is the wall thickness. Le Van and Wielgosz later improved upon Fichters beam theory by introducing finite rotation kinematics [21]. They show that the critical load to cause buckling in an inflated beam to be the following:

$$F_c \approx \frac{((E + P/S_0)I_0)\Omega^2}{1 + \Omega^2\frac{I_0}{S_0} + \Omega^2\frac{(E+P/S_0)I_0}{P+kGS_0}} \tag{20}$$

where

$$\Omega = \frac{\pi}{2l_0} \tag{21}$$

In equations (20) and (21), S_0 is cross-sectional area of the tube, k is the correction shear coefficient and l_0 is the natural length of the beam before pressurization.

Failure of a cantilevered inflated beam under transverse loading occurs when the wrinkles have propagated completely around the circumference of the tube according to membrane theory. It has been shown that the failure moment can be expressed simply as [19],[22]:

$$M_u = \pi PR^3 \tag{22}$$

The critical load at failure can be written as:

$$F_u = \frac{M_u}{L} \tag{23}$$

E. Design Considerations

The equations presented thus far can be used to design actuator geometries in order to meet specific performance goals at a variety of scales. Pressure, wall-thickness, and tube radius are the main determinants of force output, beam bending stiffness, and beam buckling stiffness. The tube radius plays an especially important role because the stress within the membrane is only directly proportional to the radius, yet the force output and critical failure forces and moments are related to the square or cube of the radius. Therefore, a modest change in radius and membrane stress can have a large impact on force output and stiffness. The maximum length of the actuator has implications on the effective stiffness of the torsion springs and the form factor of the reel. A given spiral torsion spring is only capable of rotating a maximum N_{max} number of revolutions before it is completely wound up. The radius of the reel can be increased in order to increase the maximum length of the actuator at the cost of a reduced spring force.

IV. Experiments and Results

Three experiments were conducted to examine the energy balance derived in (5) under different use cases. The three experiments are 1) set mass of air, 2) set length, and 3) set force. Throughout all of the experiments, one end of the actuator was attached to a linear slider and the other end was attached to a force gauge (American Weigh Scales SR-1). Pressure was adjusted with a manual pressure regulator (IMI Norgren R72G-2AS-007) and recorded with a pressure sensor (Honeywell 26PC). The data presented in this section was recorded using a PRA prototype containing ball bearings.

A. Set Mass of Air

During the first set of experiments, plotted in Fig. 4, a set mass of air (0-130mg) was administered to the actuator, and the external force was measured at a variety of lengths. This case exists when the actuator is stretched or compressed passively by external work acting on the actuator. To understand the actuator's performance with a constant mass of air, we will examine the relationship between 1) tensile force and length when the actuator is empty, 2) tensile force and length when the actuator is inflated, and 3) compressive force and length when the actuator is inflated.

The relationship between tensile force and length is linear when the actuator is completely deflated (Fig. 4A). The force generated in this condition is generated by the springs alone. We can extract the effective spring constant of the actuator, κ_l, as $8.6\frac{N}{m}$. Therefore, the spring force can be simplified to

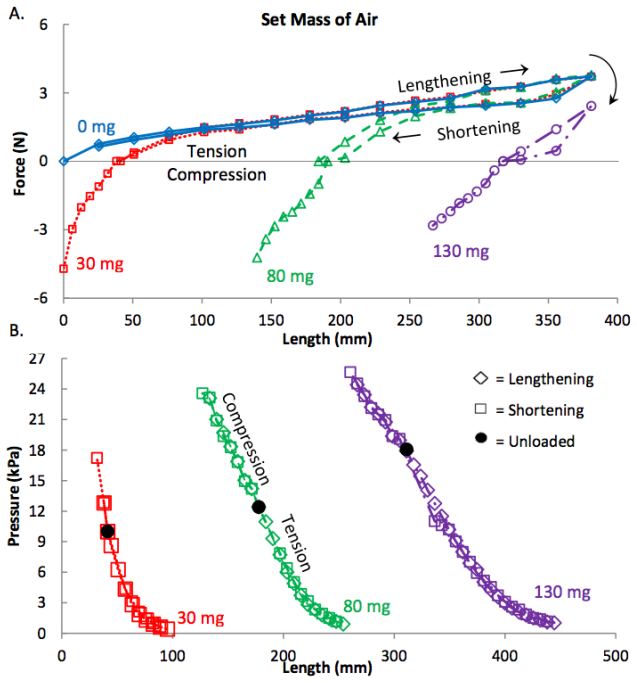

Fig. 4. The effect of length on the external force *(Top)* and the internal pressure *(Bottom)* on an actuator containing various amounts of air.

$F_{spring}(l) = \kappa_l l$. It should be noted that there exists some hysteresis in this and other data. This hysteresis could be a result of neglected terms of the energy balance discussed above.

As the amount of air in the actuator increases, the unloaded length of the actuator increases. If the actuator is extended past its unloaded length, the pressure will decrease because the effective actuator volume increases, which is inversely proportional to the pressure under the ideal gas law (Fig. 4B). The actuator length is not inversely proportional to the pressure because the cross sectional area of the tubing changes as the pressure drops. The drop in pressure reduces the force contribution from the pressurized air and the external force tends towards the spring force, which is represented in the deflated case (Fig. 4A).

Compression of the actuator will decrease the volume resulting in an increase of the pressure (Fig. 4B). This increase in pressure will produce an increase in compressive force (Fig. 4A). It can be seen that the stiffness of the actuator decreases as the mass of air increases. At longer actuator lengths, displacement of the actuator results in a smaller change in volume and pressure. Ideally, the force generated would be described by the stiffness of the plastic insert and the compression of the air. However, in the current prototype of the PRA, this is not the case as a sufficiently large force will cause the tubing to wrap back onto the reel - trapping air in the process instead of compressing it. Therefore, we do not observe an inversely proportional relationship between length and pressure under compressive loads (Fig.4B). When slipping occurs, the actuator is able to continue to operate after some of the air within the actuator is exhausted and

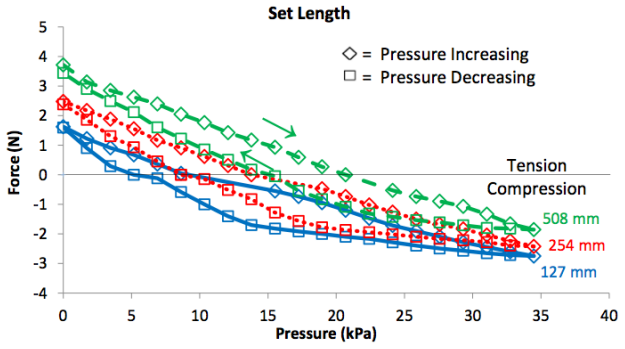

Fig. 5. The relationship between force and pressure at three different lengths.

the reel can tighten the slack tubing. Future improvements of the PRA will address this behavior.

B. Set Length

The second set of experiments fixes the length and records the force output as the pressure is incremented. This scenario is relevant in the control of robotic systems where it is often desirable to regulate a manipulator at a specified location despite disturbances. The data from this experiment are displayed in Fig. 5. At a given length, the tensile force is greatest when the pressure is zero. This tensile force is generated by the springs. Increasing the pressure while the actuators length is fixed will decrease the tensile force and increase a compressive force generated by the actuator. As such, the external force is a balance between the spring force and the force from the internal pressure. This is consistent with the result in (5). The actuators maximum force is determined by the length of the actuator. The tensile force output of the actuator increases as the length of the actuator increases because more energy has been stored inside of the springs.

C. Set Force

The third set of experiments imposes a given load upon the actuator and records the length of the actuator at various pressures. This is relevant when the actuator must move a constant load to various positions. As shown in Fig. 6, an unloaded actuator lengthens as the pressure increases. When a weight is hung below the actuator to produce a tensile force, the length of the actuator increases under constant pressure. If a compressive force is applied, the length of the actuator decreases under constant pressure. The minimum length of the actuator will increase as the tensile load increases. The hysteresis in the actuator is most apparent in this length versus pressure relationship.

D. Actuation Speed

Fig. 7 shows how the pressure and length of the actuator develop over time when powered by a pneumatic source regulated to 103 kPa. When the inlet valve is opened, the pressure and length rapidly increase. The length of the actuator extends at an average rate of 0.87 meters per second. The pressure drops immediately after the inlet valve is closed

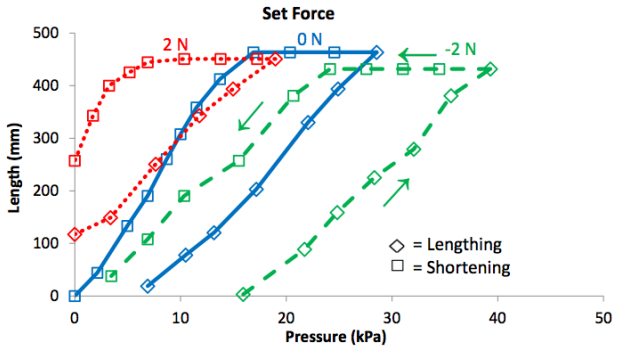

Fig. 6. The actuator length versus pressure under various loads. Tensile loading is denoted with a positive value.

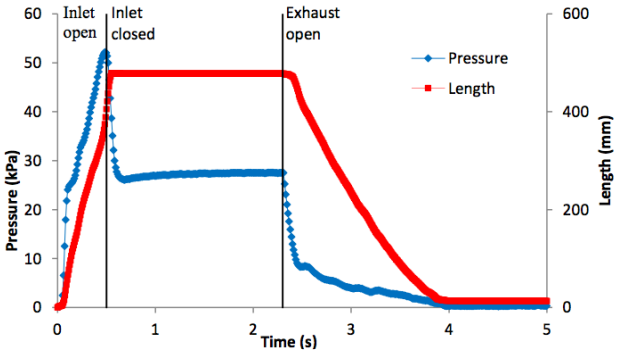

Fig. 7. The development of pressure and length over time as the actuator is inflated by a pneumatic source at 103 kPa.

but the length continues to increase for a short time. When the exhaust valve is opened the pressure suddenly drops about 70% as the air is free to leave the actuator, but the actuator length has not changed significantly. The rate of pressure loss decreases as the actuator begins to contract. The actuator contracts at an average rate of 0.28 meters per second. The pressure and length reach their equilibrium value at about the same time.

E. Beam Stiffness

Experiments were performed on inflated beams to test the theoretical failure loads caused by transverse and compressive axial loading. Fig. 8 shows that the experimental data collected for beam buckling under axial loading falls between the two models from (19) and (20). The failure load is inversely proportional to the square of the length of the beam as the models suggest. However, while the experimental data suggest increased stiffness as pressure increases, the models fail to capture that relation under the range of pressures of interest here. The experimental results for beam bending under transverse loads are aggregated in Fig. 9. The model in (23) matches the experimental data very well for both length and pressure. The bending stiffness improved by four times when these tests were repeated with the plastic insert included in the beam.

Table II aggregates some of the performance characteristics of our PRA prototypes.

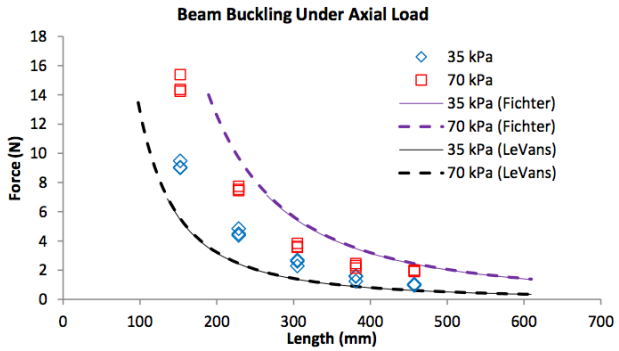

Fig. 8. Maximum axial failure loads versus beam length at two different pressures. Both Fichter's and Le Van's Model are shown here.

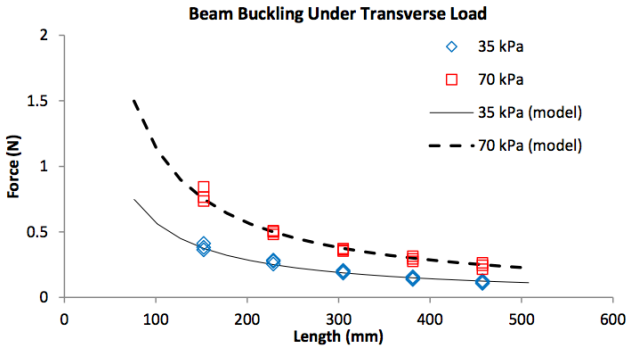

Fig. 9. Experimental and calculated maximum transverse failure loads versus beam length at two different pressures.

V. Applications

We present two applications utilizing multiple PRAs powered by a compressor generating 103 kilopascals of pressure. The first, displayed in Fig. 10, is a 3 degree-of-freedom parallel robotic arm similar to a delta mechanism [23]. By manipulating the lengths of each actuator individually, it is possible to translate the arm in three dimensions. While this mechanism is not as precise as typical rigid delta mechanisms, this robotic arm is light weight, inexpensive, and safe for interactions with humans.

The PRA was also used to construct a preliminary self-deformable robot comprised of a single tetrahedron (Fig. 11). Six actuators are joined together at nodes constructed of flexible silicone. Pressure lines are connected to three of the four nodes. This initial prototype, weighing just 2.2 Newtons, has a minimum edge length of 110 mm and a maximum edge length of 597 mm yielding a side extension ratio of 5.4:1 and a volumetric ratio of 160:1. The edge extension ratio of this preliminary robot is less than that of the PRA because some inextensible links were added

Fig. 10. Three degree of freedom parallel robot.

TABLE II

PERFORMANCE CHARACTERISTICS OF PRA PROTOTYPES

Metric	Without bearings	With bearings
Min. length [mm]	36	38
Max. length [mm]	606	540
Extension Ratio	16.8:1	14.2:1
Weight [g]	23	34
Max. Compressive Load [N]	6.4	6.4
Max. Tensile Load [N]	5.5	5.3
Max. Force to Weight Ratio	28.3:1	19.1:1
Efficiency under tension	84	85
Max. Pressure [kPa]	103	
Speed [m/s]	0.87 m/s	

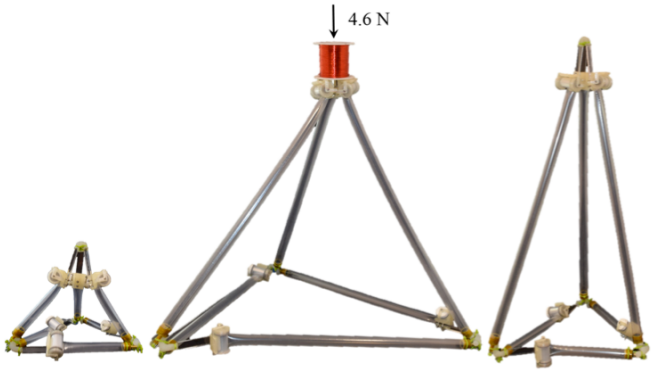

Fig. 11. Tetrahedral robot shown in three configurations. Links of this tetrahedron have an extension ratio of 5.4:1. The volume of the robot in its largest configuration is 160 times the volume of the robot in its smallest configuration.

to each actuator to ensure proper connection at the nodes without interference from adjacent actuators. This extension ratio is, nonetheless, larger than self-deformable robots in the literature [5], [6], [24], [25]. Once fully inflated, the robot can support loads greater than 4 Newtons at the top node without failure of the structure. Like other robots in the literature, this tetrahedral robot can locomote by self-deformation to achieve a punctuated rolling gait [24], [25]. Compliant linear actuator robots like this early prototype have advantages including the ability to absorb and dissipate energy from shock, a reduced control complexity of overdetermined configurations, and increased safety of interactions with people.

VI. DISCUSSION

As with any actuator, the PRA offers an inherent set of attributes that are ideal for some cases and unacceptable for others. The PRA offers large strain, low weight, low cost, ease of manufacture, compliance, and is capable of supporting tensile and compressive loading. A comparison of the PRA to other relevant actuators is aggregated in Table III. The PRA offers a unique balance of qualities that is well suited for our particular needs.

The extension ratio of the PRA is much higher than that of other soft actuators. This is due to the fact that the main structural member, the tubing, does not endure significant strain for linear expansion. While extension ratios as high as 16.8:1 have been recorded in this work, this number does not represent a theoretical maximum for PRAs. Simple modifications of the geometry and material of the PRA components could allow for significantly improved extension ratios and application across multiple scales.

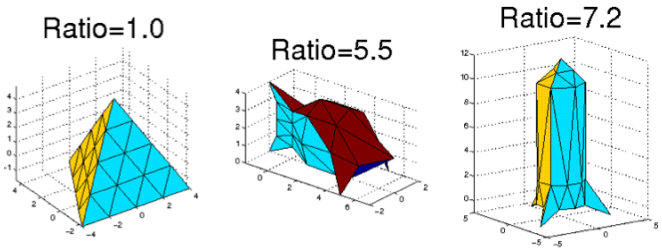

Fig. 12. A tetrahedron, fish, and rocket are be formed by the same network of linear actuators by only manipulating actuator lengths. The ratio of the longest to shortest actuator is displayed above each figure.

There are also some limitations of the actuator that should be discussed. As a pneumatic actuator, it is reliant on a high pressure source for actuation and tight seals to ensure controllability and efficiency. Unlike many other pneumatic actuators, the PRA relies on moving parts causing friction to be an inherent limitation of the actuator. Additionally, the PRA does not boast the same force to weight ratio as some of its companion pneumatic actuators. We have recorded a force to weight ratio of 28.3:1 for these PRA prototypes. However, increasing the tubing radius significantly increases the force output and stiffness of the inflated beam while only slightly increasing the weight. Therefore, much larger force to weight ratios are possible.

VII. INTEGRATION INTO SHAPE CHANGING NETWORKS

Future work on the PRA will be directed towards integration into larger scale self-deformable robotic systems. This will include the addition of length sensing for closed loop control, investigation of PRAs with varying geometries and materials, and the full integration of pneumatic and electric power sources to each actuator or group of actuators.

A key application is the ability to create networks of actuators that are capable of changing between a large variety of shapes by changing the lengths of the actuators, but leaving the network topology constant. To demonstrate this concept, the geometry of a network that consists of 120 actuators connected to 35 nodes was simulated and placed in three different configurations, as shown in Fig. 12. For each configuration, the ratio of the longest to shortest actuator is computed. For two of the three configurations shown, an extension ratio of over 5:1 is required.

In addition to acting as a shape display, large networks of connected high extension linear actuators can be used to form modular robots capable of locomotion. Past work has developed robots capable of locomotion on rough or unknown terrain by allowing a large degree of shape change [5], [6], [24], [25]. Past methods of locomotion have typically depended on punctuated rolling gaits. The high elongation ratio enabled by the PRA potentially enables a different type of locomotion. One intriguing mode of locomotion is one in which the robot turns itself inside out. An illustration of this method of locomotion is shown in Fig. 13. An extension ratio of approximately 3:1 is required to perform the gait as shown.

TABLE III
COMPARISON WITH OTHER ACTUATORS

Actuator	PRA	PAM [9]	IPAM [12]	Spiralift [13]	Spiral Zipper [14]	ZipperMast [15]
Extension Ratio	16.8:1	2:1	4:1	12.5:1	14:1	32:1
Force to Weight Ratio [N/N]	28.3:1	2000:1	1000:1	35.5:1	14.4:1	1:1
Speed	Medium	Fast	Fast	Slow	Slow	Medium
Compliant	Yes	Yes	Yes	No	No	No
Tensile Load Bearing	Yes	Yes	Yes	Yes	No	Yes
Compressive Load Bearing	Yes	No	No	Yes	Yes	Yes
Inexpensive	Yes	Yes	Yes	No	Yes	No

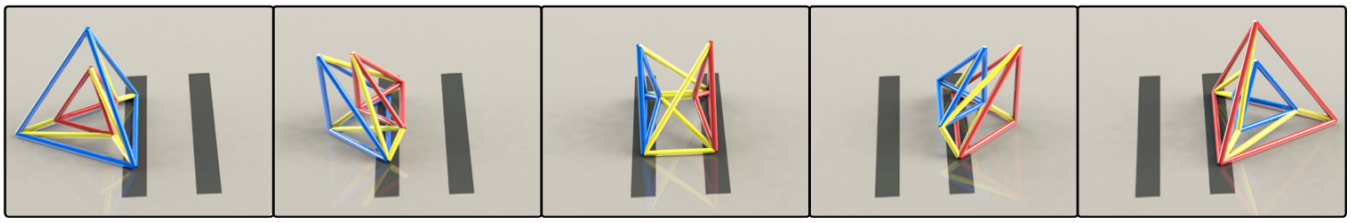

Fig. 13. A network of actuators capable of locomotion by inverting itself so that the red tetrahedron, which begins as the internal tetrahedron, ends as the external tetrahedron

VIII. CONCLUSION

We have presented a pneumatic linear actuator that is highly extensible, lightweight, capable of operating in compression and tension, compliant, and inexpensive. We have developed a model of the actuator that describes the performance of the actuator and conducted experiments that relate the length, pressure, force, and amount of air. Large scale applications of the actuator have been proposed and two small scale applications have been implemented in the form of a three degree-of-freedom delta mechanism and a tetrahedral robot.

REFERENCES

[1] M. Fujii, H. Yokoi, and Y. Kakazu, "Modeling and movement control of mobile sma-net," in *Computational Intelligence in Robotics and Automation, 2003. Proceedings. 2003 IEEE International Symposium on*, vol. 1. IEEE, 2003, pp. 253–258.

[2] C.-H. Yu, K. Haller, D. Ingber, and R. Nagpal, "Morpho: A self-deformable modular robot inspired by cellular structure," in *2008 IEEE/RSJ International Conference on Intelligent Robots and Systems*. IEEE, 2008, pp. 3571–3578.

[3] K. Stoy, A. Lyder, R. F. M. Garcia, and D. J. Christensen, "Hierarchical robots," in *IROS Workshop on Self-Reconfigurable Modular Robots*, 2007.

[4] G. J. Hamlin and A. C. Sanderson, "Tetrobot: A modular approach to parallel robotics," *IEEE Robotics & Automation Magazine*, vol. 4, no. 1, pp. 42–50, 1997.

[5] S. Curtis, M. Brandt, G. Bowers, G. Brown, C. Cheung, C. Cooperider, M. Desch, N. Desch, J. Dorband, K. Gregory *et al.*, "Tetrahedral robotics for space exploration," *IEEE Aerospace and Electronic Systems Magazine*, vol. 22, no. 6, pp. 22–30, 2007.

[6] K. Tadakuma, R. Tadakuma, K. Nagatani, K. Yoshida, M. Aigo, M. Shimojo, and K. Iagnemma, "Throwable tetrahedral robot with transformation capability," in *2009 IEEE/RSJ International Conference on Intelligent Robots and Systems*. IEEE, 2009, pp. 2801–2808.

[7] J. Rossignac, M. Allen, W. J. Book, A. Glezer, I. Ebert-Uphoff, C. Shaw, D. Rosen, S. Askins, J. Bai, P. Bosscher *et al.*, "Finger sculpting with digital clay: 3d shape input and output through a computer-controlled real surface," in *Shape Modeling International, 2003*. IEEE, 2003, pp. 229–231.

[8] F. Daerden and D. Lefeber, "Pneumatic artificial muscles: actuators for robotics and automation," *European journal of mechanical and environmental engineering*, vol. 47, no. 1, pp. 11–21, 2002.

[9] B. Tondu and P. Lopez, "Modeling and control of mckibben artificial muscle robot actuators," *IEEE control systems*, vol. 20, no. 2, pp. 15–38, 2000.

[10] C.-P. Chou and B. Hannaford, "Measurement and modeling of mckibben pneumatic artificial muscles," *IEEE Transactions on robotics and automation*, vol. 12, no. 1, pp. 90–102, 1996.

[11] G. K. Klute, J. M. Czerniecki, and B. Hannaford, "Mckibben artificial muscles: pneumatic actuators with biomechanical intelligence," in *Advanced Intelligent Mechatronics, 1999. Proceedings. 1999 IEEE/ASME International Conference on*. IEEE, 1999, pp. 221–226.

[12] E. W. Hawkes, D. L. Christensen, and A. M. Okamura, "Design and implementation of a 300% strain soft artificial muscle," in *2016 IEEE International Conference on Robotics and Automation (ICRA)*. IEEE, 2016, pp. 4022–4029.

[13] P. Gagnon and P. Laforest, "Push actuator," Oct. 24 1989, uS Patent 4,875,660.

[14] F. Collins and M. Yim, "Design of a spherical robot arm with the spiral zipper prismatic joint," in *2016 IEEE International Conference on Robotics and Automation (ICRA)*. IEEE, 2016, pp. 2137–2143.

[15] G. Woodruff, P. Muench, and G. Witus, "Zipper mast for enhanced communications and surveillance," in *SPIE Defense, Security, and Sensing*. International Society for Optics and Photonics, 2011, pp. 804 512–804 512.

[16] A. J. Daton-Lovett, "Extendible member," Apr. 17 2001, uS Patent 6,217,975.

[17] A. M. Wahl, *Mechanical springs*. Penton Publishing Company, 1944.

[18] S. P. Timoshenko and S. Woinowsky-Krieger, *Theory of plates and shells*. McGraw-hill, 1959.

[19] R. Comer and S. Levy, "Deflections of an inflated circular-cylindrical cantilever beam," *AIAA journal*, vol. 1, no. 7, pp. 1652–1655, 1963.

[20] W. Fichter, *A theory for inflated thin-wall cylindrical beams*. National Aeronautics and Space Administration, 1966.

[21] C. Wielgosz *et al.*, "Bending and buckling of inflatable beams: some new theoretical results," *Thin-Walled Structures*, vol. 43, no. 8, pp. 1166–1187, 2005.

[22] Y. He and W. Chen, "Experiment and theoretical analysis study of etfe inflatable tubes," *International Journal of Aerospace Engineering*, vol. 2014, 2014.

[23] R. Clavel, "A fast robot with parallel geometry," in *Proc. Int. Symposium on Industrial Robots*, 1988, pp. 91–100.

[24] M. Abrahantes, A. Silver, and L. Wendt, "Gait design and modeling of a 12-tetrahedron walker robot," in *2007 Thirty-Ninth Southeastern Symposium on System Theory*. IEEE, 2007, pp. 21–25.

[25] L. Zhang, S. Bi, and Y. Cai, "Design and motion analysis of tetrahedral rolling robot," in *Intelligent Robots and Systems (IROS), 2010 IEEE/RSJ International Conference on*. IEEE, 2010, pp. 502–507.